Effect of crucible rotation on the temperature and oxygen distributions in Czochralski grown silicon for photovoltaic applications

Alexandra Popescu[1], Martin P. Bellmann[2] and Daniel Vizman[1]

[1]*Faculty of Physics, West University of Timisoara Bd. V. Parvan 4, 300223 Timisoara, Romania*

[2]*SINTEF Industry, 7465 Trondheim, Norway*

Abstract

Temperature and oxygen distributions were numerically studied for the Czochralski (Cz) growth of 8" diameter silicon single crystals for photovoltaic applications. Fluctuations in the dopant concentration (striation pattern) in the grown crystal obtained by Lateral Photovoltage Scanning (LPS) technique seems to be better correlated with simulated temperature fluctuations near the solid-liquid interface than with oxygen concentration oscillations. From the transient simulations of different crucible rotation rates, 2, 4, 6 and 8 rpm, it is indicated that the average oxygen melt concentration first decreases with increasing rotation rate and later increases. This suggests that a critical rotation rate exists where the oxygen concentration below the solid-liquid interface increases with increasing rotation rate. When comparing the temperature and oxygen distributions in the melt it was found that oxygen is more sensitive to changes in the rotation rate than the temperature.

1. Introduction

Due to excellent material properties, single-crystalline silicon is the technology with the highest potential for enabling widespread deployment of photovoltaic energy. However, the performance is limited through the presence of oxygen. In Czochralski (Cz) single-crystal growth the dissolution of the quartz crucible at high temperatures contaminates the melt with oxygen, which is then reflected in the growing ingot. Most solar cells today are made from boron doped silicon (p-type). The ultimate efficiency potential of each material is limited by the presence of defects and impurities, which reduce the minority carrier lifetime. In Cz-silicon, the carrier lifetime is dominated by the well-known boron-oxygen defect [1,2]. The impurities are incorporated in melt-grown crystals at solid-liquid interface. In the longitudinal sections of these crystals it can be observed the so-called striations which reveal the pattern of the impurities incorporated in crystals

and display the shape of solid-liquid interface. In general, the occurrence of striations in melt growth is mainly caused by fluctuations of the growth rate V, which influences the incorporation of the solute according to the segregation effect [3]. Unsteady heat transfer in melt growth generates fluctuations of the growth rates. Therefore, it is expected that striations pattern to be influenced not only by the impurities distribution in the melt but also by the temperature fluctuations.

Melt convection is acknowledged to be a very important factor in the field of crystal growth. It can be stated that the control of convective transport is one of the key parameters for the control of material properties and crystal yield in industrial production of Cz-silicon crystals. Convective flows are contributing to the heat transfer and thus controlling the rate of solidification, which is very high (tens of mm/h) in the case of silicon for photovoltaic applications in comparison with the case of silicon for electronic applications.

The resulting temperature field in the vicinity of the solid-liquid interface is affecting its shape and therefore the generation of thermal stress and the formation of dislocations. Convection also controls the species/impurity transport in the melt. It affects the dissolution rate of crucible materials, the entry and evaporation of impurities from, respectively to, the gas phase via the melt free surface. Furthermore, in a complex interaction of both heat and species transport, convection strongly influences the morphology and stability of the solid-liquid interface.

Today, various numerical models are available for the calculation of temperature distribution and melt convection in a Cz method for growth of silicon [3 - 7]. For the validation of numerical results, a comparison to experiments for large silicon melts is necessary, although it is rather difficult to obtain sufficiently detailed experimental data with all parameters necessary for a numerical simulation. There are only a few contributions that make a direct comparison with the experimental results [3, 4]. They showed a good qualitative agreement between the time dependent characteristics of temperature in monitor points under the solid-liquid interface obtained in simulations and a real growth experiment. On the other hand, it is also well known that the temperature oscillations under the solid-liquid interface are generating striations pattern in the grown crystal. It is the aim of this work to perform three dimensional direct numerical simulations (DNS) of convection in a Cz configuration and to correlate the image analysis of the striation pattern in the crystals obtained by Lateral Photovoltage Scanning (LPS) - technique with the

temperature and oxygen concentration in the melt close to the solid-liquid interface. Furthermore, the influence of crucible rotation on the temperature and oxygen distributions will be investigated.

2. Experimental

The crystal growth experiment was carried out using an industrial scale Cz-furnace FerroTec CZ2208. A high-purity quartz crucible was charged with 60 kg of electronic grade polysilicon and a crystal with a diameter of 8" was grown from the melt (Figure 1). The crystal was doped with phosphorus to achieve p-type conductivity. Longitudinal samples were taken from the center of the ingot and mirror polished to reveal striation patterns with the LPS method. By scanning the laser spot over the sample surface and storing the LPS signal, a two-dimensional picture of the doping striations is obtained. For the LPS measurements an incident light beam with a wavelength of 830 nm was used. The spacing between each measured point was set to 50 µm and the time constant to 20 ms.

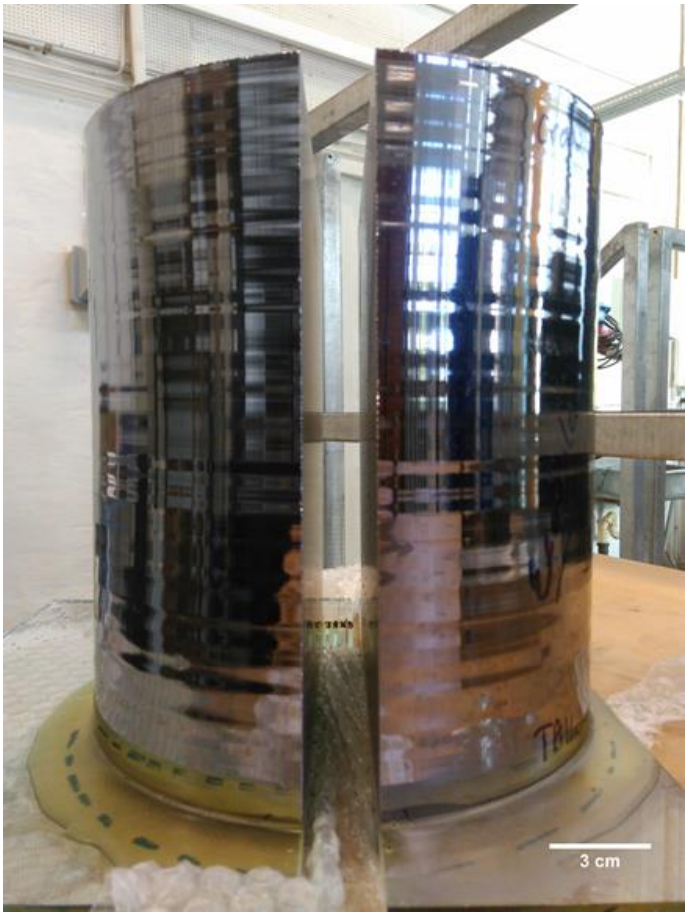

Figure 1. Part of the grown 8" silicon single crystal

Oxygen contributes to the resistivity in the form of thermal donors [8]. Therefore the striations pattern is a picture of how impurities (mainly phosphorous and oxygen in our case) are incorporated through segregation in the crystals. One should also notice that the segregation process is strongly dependent by the local growth velocity (different by the pulling rate) which is strongly dependent by the temperature fluctuations in the melt. So that it is expected that also temperature instabilities should contribute to the striations pattern.

3. Problem description

To study the temperature and oxygen transport phenomena in the Cz configuration, a 3D numerical model has been developed using the STHAMAS3D software. The computational domain consists of a 200 mm cylindrical shaped crystal with a height of 40 mm and a hemispherical shaped crucible with 490 mm in diameter and 118 mm in height. The geometry, as used in the 3D simulation is shown in Figure 2.

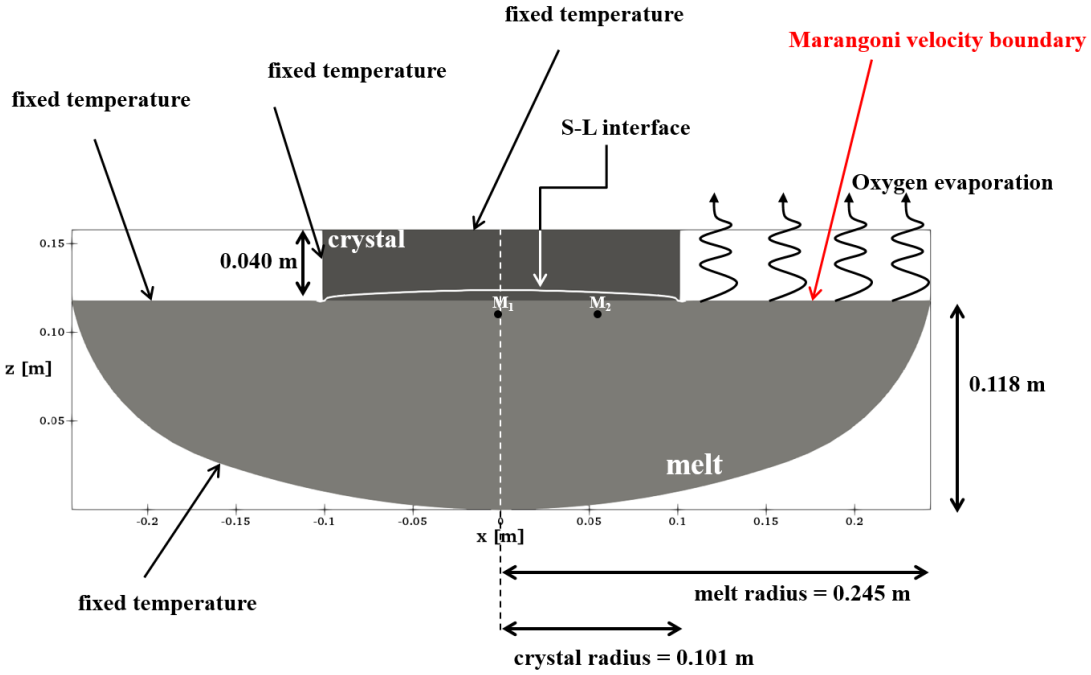

Figure 2. Schematic representation of the 3D numerical model

The crystal length was fixed during the simulation so that the incorporation of impurities in the crystal was not considered. The study was focused on the melt convection in order to understand the temperature and oxygen behavior over time.

The mathematical model used to describe the melt flow of an incompressible fluid is given by the Navier-Stokes equations:

- the mass conservation:

$$\nabla \vec{v} = 0$$

- momentum conservation:

$$\rho\left(\frac{\partial \vec{v}}{\partial t} + \vec{v}\nabla\vec{v}\right) = -\nabla p + \mu\nabla^2\vec{v} + \vec{F}$$

- heat transport equation:

$$\rho C_p \frac{\partial T}{\partial t} = \nabla(k\nabla T) - \rho C_p \vec{v}\nabla T$$

where $\vec{v}$ is the fluid velocity, ρ the density of the fluid, p is the pressure, C_p is the heat capacity and k is the thermal conductivity.

The force term in the momentum equation is given by the Boussinesq approximation used, in the numerical modeling, for buoyancy driven flows:

$$\vec{F} = -\rho T_{ref}\vec{g}\left(T - T_{ref}\right)$$

where $\vec{g}$ is the gravitational acceleration and T_{ref} is a reference temperature.

To take into account the diffusion of Oxygen (O) into the silicon melt, the O transport equation is also considered in the numerical modeling:

$$\frac{\partial c}{\partial t} = \nabla(D_O\nabla c) - \vec{v}\nabla c$$

with c being the O concentration and D_O is the O diffusion coefficient in the melt, fixed at $5\cdot10^{-8}$ m^2/s.

The temperature boundary conditions are imported from a 2D axisymmetric global Cz furnace model, performed on a geometry with similar dimensions. In order to specify the temperature profile extracted from the 2D simulation, Dirichlet boundary conditions were imposed on the crucible walls, crystal lateral walls and crystal top, as well as on the free melt surface. At the melt free surface Maragoni convection was also taken into consideration, with a Marangoni coefficient of 10^{-4} N/K·m.

The O concentration boundary conditions were set:

- on the crucible walls as the O equilibrium concentration, $C_O(T)$, given in [9]:

$$C_O(T) = 5 \cdot 10^{22} \cdot \frac{1.32 \cdot \exp(-7150/\mathrm{T} - 6.99)}{1 - 1.32 \cdot \exp(-7150/\mathrm{T} - 6.99)} [atoms/cm^3]$$

- at the melt free surface, as a function of the O evaporation coefficient [9]:

$$\varepsilon(T) = 5.1952 \cdot 10^7 \cdot e^{-\frac{4.1559 \cdot 10^4}{T}}$$

At the solid-liquid interface the latent heat production is taken into consideration:

$$k_S \frac{\partial T}{\partial n} - k_L \frac{\partial T}{\partial n} = \rho_S v_g \Delta H$$

where k_s and k_L are the thermal conductivities of the silicon crystal and melt, respectively, v_g is the growth rate and ΔH is the latent heat. The pulling velocity of the crystal is fixed at 1.2 mm/min or 7.2 cm/h.

Also, at the crystal-melt interface a no-flux condition has been imposed for oxygen:

$$\frac{\partial C_O}{\partial n} = 0$$

To determine the position and shape of the solid−liquid interface, a phase tracking procedure was used; that is, after each time step, the grid is deformed in such a way that the boundary between melt and solid fits to the melting temperature.

The material properties of Silicon melt and crystal used in the numerical modeling are given Table 1.

Parameter	**Value**		**Unit**
	Si crystal	***Si melt***	
Thermal conductivity, k	22 [10]	66.5 [11]	W/m·K
Specific heat, c_p	927	911[11]	J/kg·K
Density, ρ	2330 [12]	2570 [11]	kg/m^3
Latent heat, ΔH		$4.6 \cdot 10^{-9}$	J/m^3
Melting temperature, T_m	1685 [11]		K
Viscosity, η	-	0.0008 [13]	kg/m·s
O diffusion coefficient	-	$5 \cdot 10^{-8}$[13]	m^2/s

Table 1. Material properties of Silicon

All the numerical modeling has been done with the STHAMAS3D software that has already been validated for Czochralski and Direct Solidification silicon growth [5,14]. The computational domain is divided into 11 blocks with a grid refinement at the walls to solve the boundary layers. The computational grid has 485760 control volumes that are sufficient to describe

the main features of the fluid flow. 3000 s of real time, with a time step of 0.1s, have been simulated.

In our analysis, we considered two monitor points situated in the melt at 5 mm below the solid-liquid interface, as seen in Figure 2. Monitor point 1 (M1) is positioned on the crystal axis and monitor point 2 (M2) is placed at 5.9 cm lateral form the axis. An important issue for the quality of the numerical simulations is the choice of the grid. In order to see the influence of the grid levels on the solution we performed calculation for two grid levels (286625 CV and 485760 CV). In Figure 3(a) the resulting temperature fields along a horizontal line situated at 5 mm below the S-L interface is presented. It can be observed that the results are similar. In addition, a very good agreement can be observed in temperature fluctuations in monitor point M2 (average temperature in M2 is 1686.97 K for the fine grid and about 1687.13 K for the coarse grid) (Figure 3(b)) and power spectral density (Figure 3(c)). Consequently, we consider that the grid level does not have a strong influence for a grid level over 300000 CVs. In the calculations, we used the fine grid, which is the higher level we can compute on a workstation.

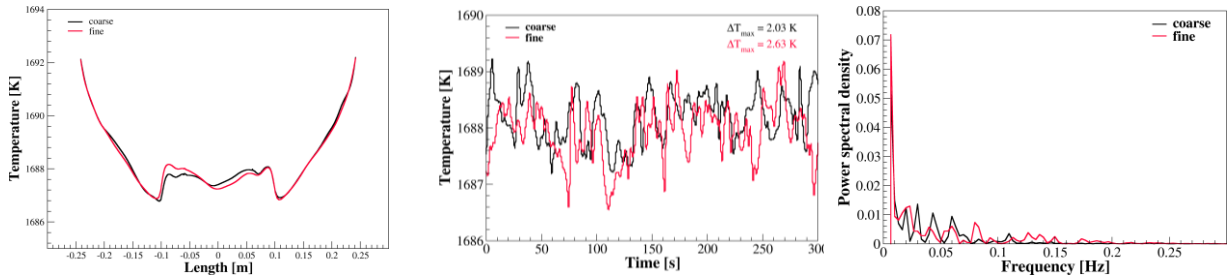

(a) (b) (c)

Figure 3. (a) Temperature profile across a horizontal line situated at 5 mm below the S-L interface (b) temperature fluctuations in monitor point M2. (c) power spectral density in monitor point M2

4. Results and discussions

A reference case with a crucible rotational rate (ω_{cru}) of 6 rpm and a crystal rotation rate (ω_{cry}) of 10 rpm has been taken into consideration. The results from the numerical modeling have been compared with experimental results obtained from a LPS that reveals striations on a silicon slab that has been analyzed, as seen in Figure 4.

In order to evaluate the time evolution of the striations an image analysis using the ImageJ software was performed for the LPS result along a vertical line (Figure 4) corresponding to a monitor point close to the crystal axis (M1). The pixel intensity along this line is presented in Figure 5(a).

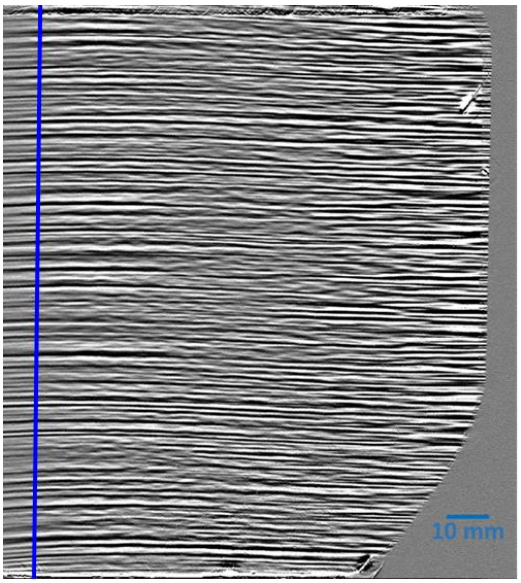

Figure 4. Crystal striation in a vertical section

Temperature and oxygen concentrations fluctuations over 3000s were also analyzed in a monitor point M1 situated in the melt at crystal axis and 5 mm under the free surface (Figure 5(b) and 5(c)).

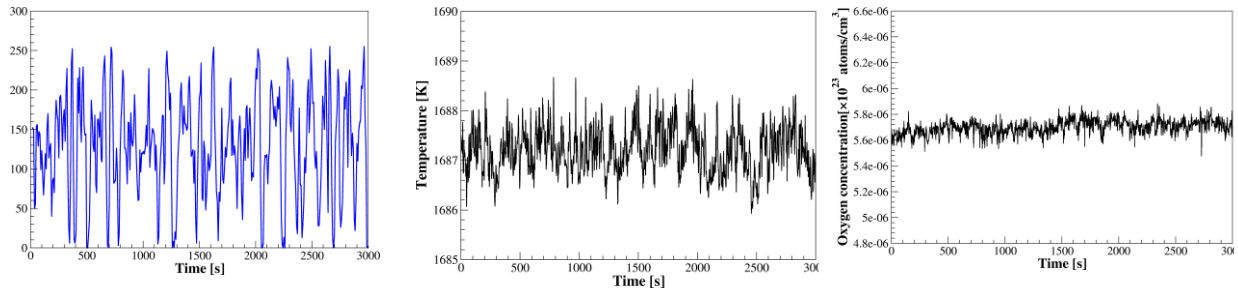

(a) (b) (c)

Figure 5.Time evolution of the (a) pixel intensity; (b) temperature and (c) oxygen concentration in a monitor point situated close to the crystal axis, 5 mm under the free surface (for (b) and (c))

In order to determine if there is a correlation between the time evolution of the striations, temperature and oxygen concentration, the histograms for all three-time evolution processes are presented in Figure 6. As we mentioned in introduction, the striations pattern is the result of the impurities trapped in the crystal at S-L interface through the segregation process. Therefore, the striations pattern is influenced by a superposition of the temperature fluctuations (which generate a growth velocity fluctuation) and impurities fluctuations near S-L interface (mainly oxygen in our case). From figure 6 it can be observed that the histograms for pixel intensity and temperature (Figures 6 (a) and (b)) are more symmetric (unimodal) than the histogram for oxygen concentration (Figure 6 (c)), which is skewed left. Therefore, it can be concluded that temperature oscillations seem to have a stronger fingerprint on the striations pattern.

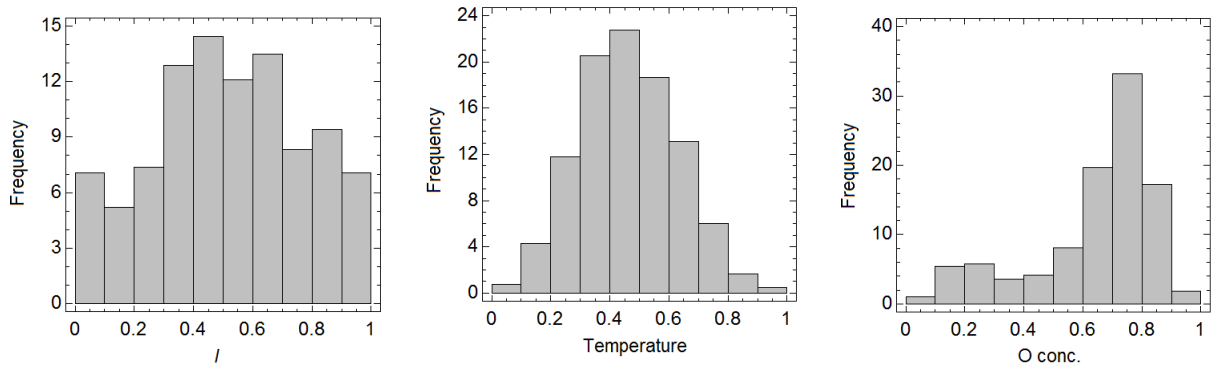

(a) (b) (c)

Figure 6. Histograms for the (a) pixel intensity; (b) temperature and (c) oxygen concentration in a monitor point situated close to the crystal axis and 5 mm under the free surface (for (b) and (c))

To understand the influence of crucible rotation on the crystal quality we studied the influence of crucible rotation on the temperature and oxygen time evolution. Three other values for crucible rotation have been considered: ω_{cru} = 2, 4 and 8 rpm in addition to the reference case. The crystal rotation rate was fixed at 10 rpm for all the studies. Numerical simulations have been performed with the same temperature boundary conditions. In a real experiment, the heater power is adjusted with the crucible rotation change, but in our study, we consider of interest to understand the sole influence of the crucible rotation on the melt convection.

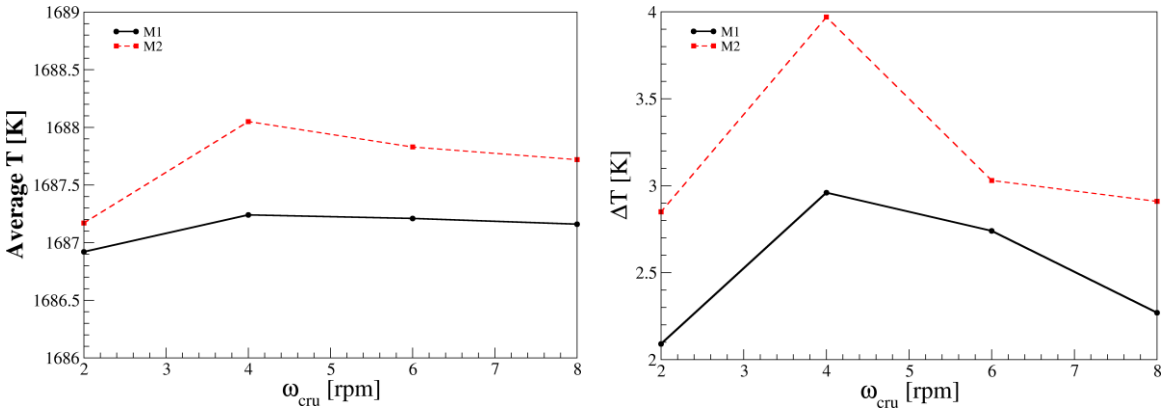

(a) (b)

Figure 7. Average temperature variation with crucible rotation in monitor points (a); amplitude of temperature fluctuations variations with crucible rotation in monitor points (b)

From Figure 7(a) it can be observed that the average temperature in both monitor points is barely affected by the crucible rotation. However, the amplitude of temperature fluctuations is stronger affected by the crucible rotation. First, it can be observed that the temperature fluctuations are more intense near the crystal edge (M2 curve in Figure 7(b)) than at the center of the melt (M1 curve in Figure 7(b)), mainly because the center of the melt is less directly affected by crystal and crucible rotations (centrifugal forces are weaker in the central part of the melt). The increase of crucible rotation generates at first an increase in temperature fluctuations and, after reaching a critical value, it generates a decrease in temperature fluctuations (Figure 7(b)).

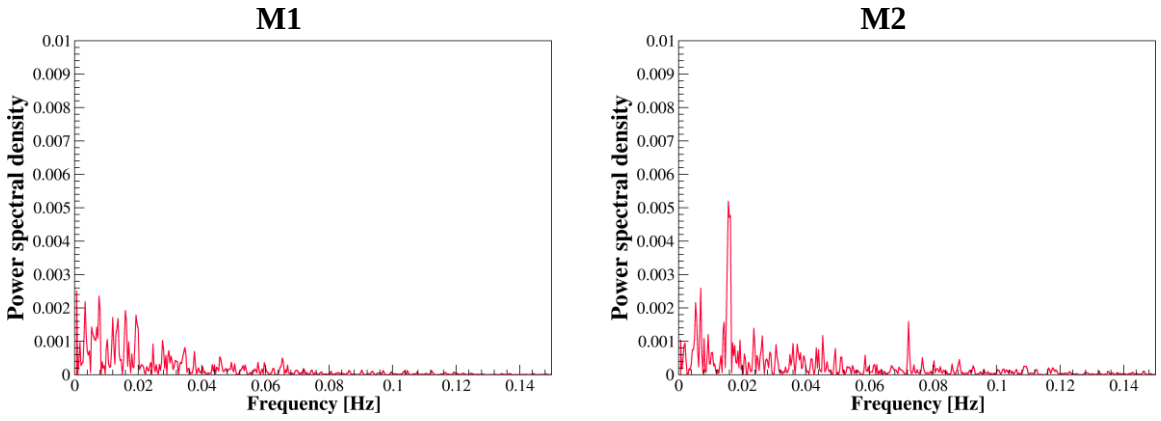

(a) (b)

ω_{cru} = 2 rpm

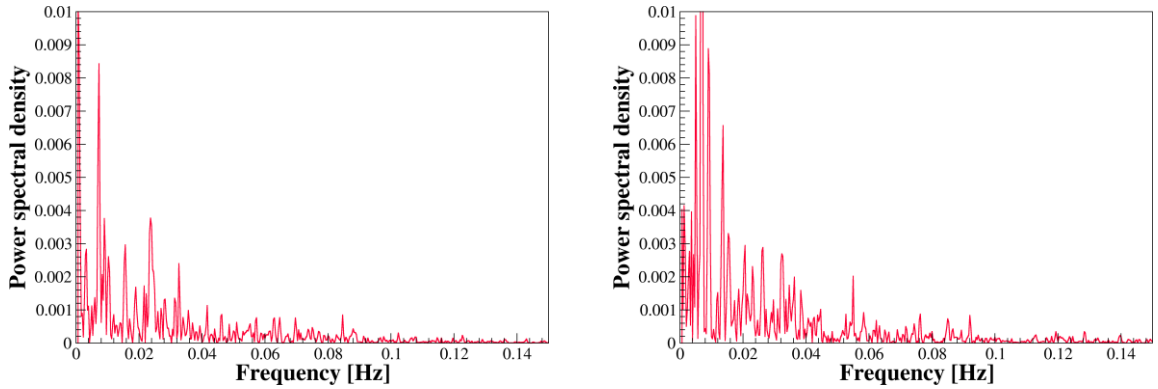

(c) (d)

ω_{cru} = 4 rpm

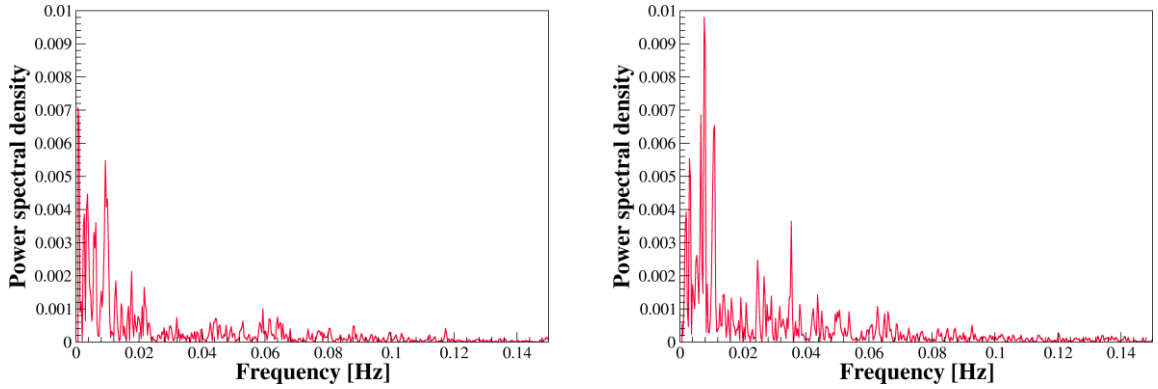

(e) (f)

ω_{cru} = 6 rpm

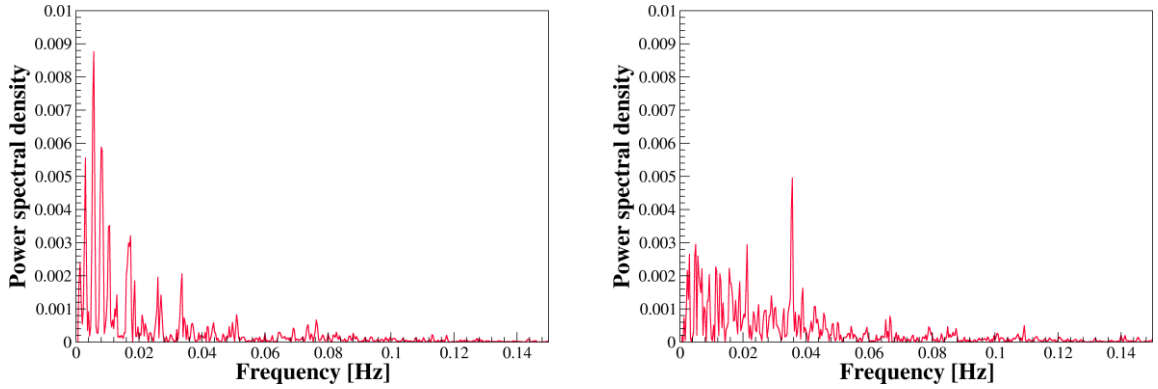

(g) (h)

ω_{cru} = 8 rpm

Figure 8. Power spectral density corresponding to temperature fluctuations for two monitor points and various crucible rotations.

Further information about the flow state comes from the evaluation of Power Spectral Density (PSD) corresponding to temperature fluctuations shown in Figure 8. One cannot observe any dominant single frequency peak related to the crystal or crucible rotation. This shows us that the region under the crystal is dominated by buoyancy convection. For the lowest crucible rotation rate (2 rpm), the power is, somehow, uniformly distributed over the frequencies for the monitor point M1, which denotes a soft turbulence flow. With the increase of the crucible rotation rate (4, 6, 8 rpm) more power is concentrated at lower frequencies (less than 0.02 Hz) and there is a sharper decrease of power towards the higher frequencies, which indicates a more turbulent flow than in the case of 2 rpm.

It can be concluded that the melt flow behavior at the crystal axis under the solid-liquid interface (M1) is less influenced by the increase of crucible rotation (PSD for M1 and crucible rotation 4, 6, 8 rpm are very similar – see Figures 8(c), (e), (g)). In comparison to M1, in the spectrum for monitor point M2, higher frequencies occur. For a crucible rotation rate of 2 rpm, for M2 the power is also uniformly distributed, with a significant peak around 0.016Hz, which denotes furthermore a weak turbulence. For the crucible rotations of 4 rpm and 6 rpm more power is concentrated at lower frequencies (less than 0.02 Hz) and there is also a sharper decrease of power toward the higher frequencies (as in the case for M1), which indicates a more turbulent flow than in the case of 2 rpm (see Figures 8 (d), (f)). Contrary to the flow behavior in M1, the melt flow near the crystal edge (M2) is again less turbulent, with the power more uniformly distributed and with a significant peak around 0.036Hz. This behavior at higher crucible rates is due to a higher centrifugal force which damps the flow convection.

The oxygen distribution is another key element for the quality of the grown crystal. Therefore, we studied the oxygen distribution in relation with crucible rotation. The oxygen level both at the crystal axis and at the edge of the crystal is first decreasing with the increase of crucible rotation rate and then increasing (see Figure 9(a)). This suggests that there is a critical crucible rotation from where the O-concentration under the crystal increases with the crucible rotation. Comparing temperature and oxygen concentration field (Figure 7(a) and Figure 9(a)), it can be observed that oxygen concentration is more sensitive to the crucible rotation than the temperature field.

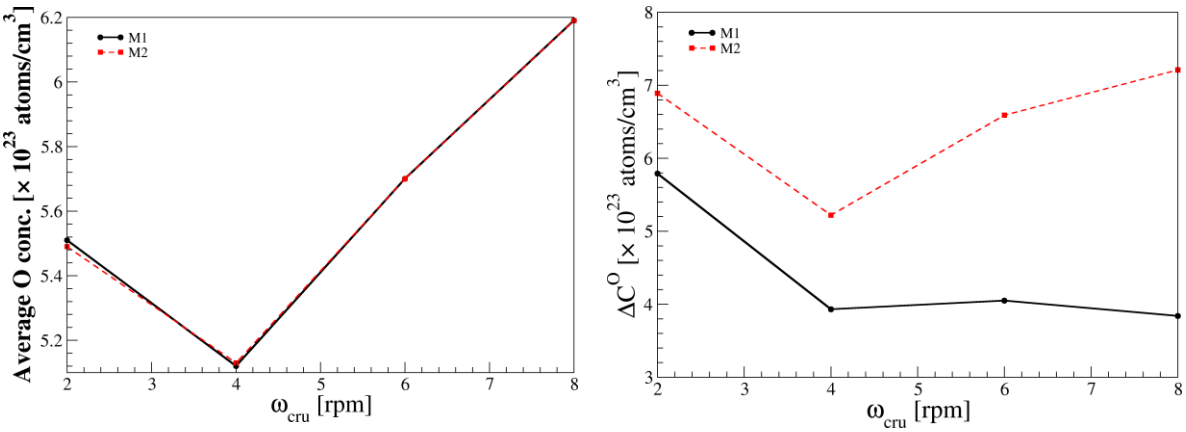

(a) (b)

Figure 9. Average oxygen concentration variation with crucible rotation in monitor points (a); amplitude of oxygen concentration fluctuations variations with crucible rotation in two monitor points (b).

The amplitude of oxygen concentration variation is higher at the crystal edge than at the crystal axis (Figure 9(b)). For higher crucible rates the amplitude of oxygen concentration fluctuations is slightly increasing with the crucible rate as opposed to the amplitude of temperature fluctuations which is decreasing (Figure 7(b)). It is also important to note that the oxygen concentration has a homogeneously radial distribution under the solid-liquid interface as it can be observed from the oxygen distribution along a line in the radial direction fixed at 11.3 cm from de crucible bottom (Figure 10). The same behavior can also be observed in Figure 9(a). In comparison, temperature field is not so homogeneous under the S-L interface with a difference of about 1K between symmetry axis and crystal edge (Figure 7(a)).

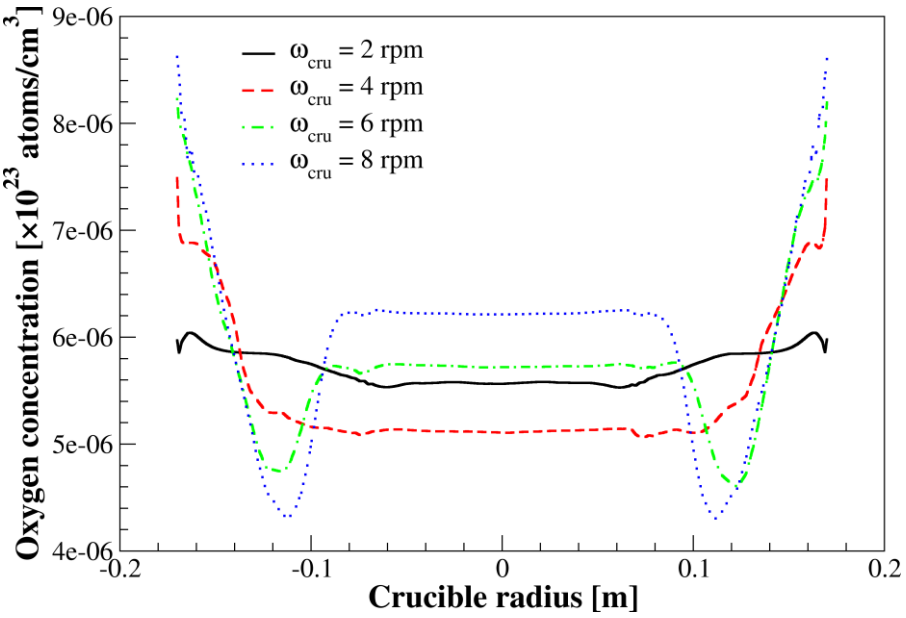

Figure 10. O concentration distribution on a line fixed at 11.3 cm from de crucible bottom

In order to understand the behavior of oxygen concentration variation with the crucible rotation, time-averaged (over 800s) O-concentration distribution is represented in a vertical section (xOz) for every crucible rotation (Figure 11). It can be observed that, for a low crucible rotation rate, oxygen concentration is more uniformly distributed in the melt due to diffusion and convection. Once with the increase of crucible rotation, the centrifugal force increases and the main buoyant convection role is pushed to the sidewalls. So, the oxygen generated at the crucible wall cannot travel as easy toward the center of the melt and will accumulate near the walls. In this region the oxygen concentration will constantly increase with the crucible rotation. The oxygen level in the center part of the melt, under the S-L interface, is generated by both convection and diffusion. A slight increase in the crucible rotation rate (4 rpm) will prevent the oxygen to travel, by convection, under the S-L interface, so there is a decrease of concentration in the center, under the S-L interface, while the O concentration increases near the crucible walls. By further increasing the crucible rotation rate, the oxygen concentration near the crucible wall will increase even more and the diffusion process to the central part of the melt will intensify which leads to an increase of oxygen level under the S-L interface.

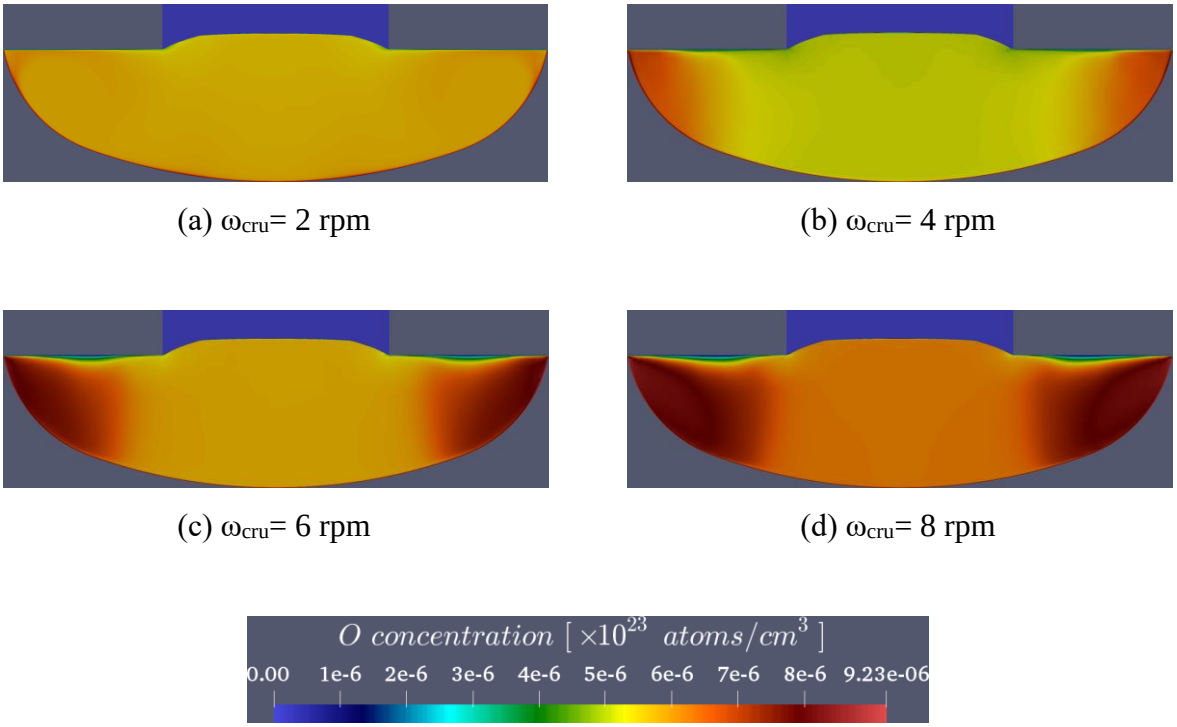

Figure 11. Time averaged oxygen concentration field for different values of the crucible rotation rate

5. Conclusions

Numerical simulations and experimental investigations were performed in order to understand the melt flow characteristics in the Czochralski growth of 200 mm diameter silicon crystals for photovoltaic applications. The simulation results of temperature and oxygen concentration fluctuations under the S-L interface and image analysis of the striations pattern in the crystals obtained by LPS technique were compared. Striations pattern seems to be better correlated with simulated temperature fluctuations near the solid-liquid interface than with oxygen concentration oscillations.

In order to study the influence of crucible rotation on the temperature and oxygen concentration distribution, four crucible rotation rates were considered. Temperature boundary conditions for the local three-dimensional numerical simulations were taken from a two dimensional global simulation.

Information about the flow state were obtained from evaluating the amplitude of temperature fluctuations and from the corresponding Power Spectral Density. First, it can be observed that the temperature fluctuations are more intense near the crystal edge than at the center of the melt, mainly because the central part of the melt is less directly affected by crystal and crucible rotation, due to lower centrifugal force. The increase of crucible rotation generates, at first, an increase in temperature fluctuations and, after reaching a critical value, it generates a decrease in temperature fluctuations.

The melt flow behavior at the crystal axis under the S-L interface is dominated by buoyancy and is less influenced by the increase of crucible rotation.

Contrary to the central part, the melt flow near the crystal edge is strongly affected by the crucible rotation such that, at first, the increase of the crucible rotation rate (2 – 6 rpm) leads to an increase in the turbulence level of the melt convection. For a higher crucible rotation rate (8 rpm), the melt becomes once again less turbulent due to a higher centrifugal force that damps the flow convection.

Regarding the O-concentration distribution, it was found that the concentration has a homogeneously radial distribution under the solid-liquid interface. Also, it was concluded that by increasing the crucible rotation rate, first the level of oxygen concentration under the S-L interface decreases and, from a critical crucible rotation rate, the O-concentration increases. It was shown that, in comparison to the temperature field, the oxygen concentration is more sensitive to the crucible rotation rate variations. For higher crucible rotation rates, the amplitude of oxygen concentration fluctuations is slightly increasing with the crucible rotation rate in opposite to the amplitude of temperature fluctuations, which is decreasing.

6. Conflicts of interest

There are no conflicts of interest to declare.

7. Acknowledgments

This work was supported by a grant of Ministry of Research and Innovation, CNCS-UEFISCDI, project number PN-III-P1-1.1-TE-2016-0416, within PNCDI III.

8. References

1. J. Schmidt - *Light-Induced Degradation in Crystalline Silicon Solar Cells*, ***Solid State Phenomena*** **95-96**, 187-196 (2004).
2. J. Schmidt, K. Bothe - *Structure and transformation of the metastable boron- and oxygen-related defect center in crystalline silicon*, ***Physical Review B*** **69**, 024107 (2004).
3. J. Friedrich, W. von Amon, G. Mueller, *Handbook of Crystal Growth: Bulk Crystal Growth*, Pages 46-98, Elsevier, (2014)
4. I. Yu Evstratov, et al. - *Global model of Czochralski silicon growth to predict oxygen content and thermal fluctuations at the melt–crystal interface*, ***Microelectronic Engineering*** **56** (1–2), 139-142 (2001).
5. D. Vizman, O. Gräbner, G. Müller - *Three-dimensional numerical simulation of thermal convection in an industrial Czochralski melt: comparison to experimental results*, ***Journal of Crystal Growth*** **233**, 687-698 (2001).
6. B. Gao and K. Kakimoto - *Global simulation of coupled carbon and oxygen transport in a Czochralski furnace for silicon crystal growth*, ***Journal of Crystal Growth*** **312**, 2972-2976 (2010).
7. T. H. T. Nguyen, J. C. Chen, C. Hu, C. H. Chen - *Numerical simulation of heat and mass transfer during Czochralski silicon crystal growth under the application of crystal-crucible counter- and iso-rotations*, ***Journal of Crystal Growth*** **507**, 50-57 (2019).
8. K. Wada - *United model for formation kinetics of oxygen thermal donors in silicon*, ***Physical Review B*** **30**, 5884 (1984).
9. S. Hisamatsu, H. Matsuo, S. Nakano, K. Kakimoto - *Numerical analysis of the formation of $Si_3N_4$and Si_2N_2O during a directional solidification process in multicrystalline silicon for solar cells*, ***Journal of Crystal Growth*** **311**, 2615-2620 (2009).
10. K. Ohsaka, S. K. Chung, W. K. Rhim, and J. C. Holzer - *Densities of Si determined by an image digitizing technique in combination with an electrostatic levitator*, ***Applied Physics Letters*** **70**, 423-425 (1997).
11. T. Jung, J. Seebeck, J. Friedrich - *Combined global 2D–local 3D modeling of the industrial Czochralski silicon crystal growth process*, ***Journal of Crystal Growth*** **368**, 72-80 (2013).
12. C. J. Glassbrenner, Glen A. Slack - *Thermal Conductivity of Silicon and Germanium from 3°K to the Melting Point*, ***Physical Review*** **134**, A1058 (164).

13. V. V. Kalaev, I. Yu. Evstratov, Yu. N. Makarov - *Gas flow effect on global heat transport and melt convection in Czochralski silicon growth,* ***Journal of Crystal Growth*** **249**, 87-99 (2003).
14. A. Popescu, D. Vizman, - *Numerical Study of Melt Convection and Interface Shape in a Pilot Furnace for Unidirectional Solidification of Multicrystalline Silicon,* ***Crystal Growth and Design 12***, 320-325, (2012).